Electronic supplementary materials *Mendeleev Commun.*, 2020, **30**, 719–721

Photoinduced solid-state isomerization and structural characterization of a nitro–nitrosyl ruthenium complex with 3-cyanopyridine

Artem A. Mikhailov, Denis P. Pishchur, Natalia V. Kuratieva and Gennadiy A. Kostin

IR spectra were recorded using KBr pellets on a VERTEX 80v-spectrometer. GS to MS1 photo-isomerization and reversed MS1 to GS transformation were studied in a cryostat cell at a temperature range of 80–220 K. The pellet was mounted onto the cryostat cell, cooled to 80 K, and irradiated by a blue laser (445 nm, 100 mW cm^{-2}) to obtain MS1 isomer. The cryostat cell was then heated to the required temperature and the isothermal kinetics were monitored at the MS1 band (1761 cm^{-1}).

UV–vis spectrum of the $[RuNO(3\text{-}CN\text{-}Py)_2(NO_2)_2OH]$ complex was recorded on a PG Instruments T60 UV–vis single-beam spectrophotometer in a 1 cm cell using acetonitrile as a solvent. The absorbance of the pure solvent was taken in account.

A differential scanning calorimeter NETZSCH DSC 204 F1 Phoenix was used to study the kinetics and thermal effects accompanying the reverse MS1 to GS process. First, the sample was cooled to 80 K and irradiated at 445 nm. The DSC measurements of the irradiated samples (the masses were 1–3 mg) were taken in open aluminum crucibles using the heat flow measurement method at a heating rates of 9, 12 and 15 K min^{-1} under a 25 mL min^{-1} Ar flow. To investigate the decay of MS1, the irradiated sample was heated to 275 K. The sensitivity calibration of the sample carrier sensors and temperature scale graduation were determined from melting and crystal-to-crystal transition measurements of standard samples (C_6H_{12}, Hg, KNO_3, and In). The experimental data were processed using Netzsch Proteus Analysis software.

Density functional theory calculations of were performed using the ADF2017 package [1]. For geometry optimization of the complexes, the hybrid B3LYP functional [2] and the triple-z-quality with one polarization function (TZP) basis set [3] were used. A closed-shell electron configuration was employed for the complex. The scalar relativistic zero-order regular approximation (ZORA) [4] for the Hamiltonian was applied. The mean absolute deviation of all bond length of the calculated and experimental structure is 0.024 Å. The widely applied B3LYP functional was selected due to the good agreement between calculated structures of ruthenium complexes and experimental data in previous investigations [5]. Computed UV-vis spectra were generated for optimized structures using the same level of theory with COSMO solvation method with acetonitrile as solvent [6]. The Davidson method was used for the first 50 electronic excitations.

Table S1. Crystal data and structure refinement for $[RuNO(3\text{-}CN\text{-}Py)_2(NO_2)_2OH]$.

Empirical formula	$C_{12}H_9N_7O_6Ru$
Formula weight	448.33
Temperature/K	150
Crystal system	orthorhombic
Space group	$P2_12_12_1$
a/Å	9.9129(3)
b/Å	12.1195(4)
c/Å	13.7976(4)
α/°	90
β/°	90
γ/°	90
Volume/$Å^3$	1657.64(9)

Z	4
ρ_{calc}g/cm^3	1.796
μ/mm^{-1}	0.993
F(000)	888.0
Crystal size/mm^3	0.13 × 0.1 × 0.08
Radiation	MoKα (λ = 0.71073)
2Θ range for data collection/°	4.474 to 55.042
Index ranges	$-12 \leq h \leq 9$, $-15 \leq k \leq 13$, $-17 \leq l \leq 17$
Reflections collected	10853
Independent reflections	3734 [R_{int} = 0.0291, R_{sigma} = 0.0354]
Data/restraints/parameters	3734/0/239
Goodness-of-fit on F^2	1.034
Final R indexes [I>=2σ (I)]	R_1 = 0.0255, wR_2 = 0.0527
Final R indexes [all data]	R_1 = 0.0289, wR_2 = 0.0540
Largest diff. peak/hole / e Å^{-3}	0.67/-0.49
Flack parameter	0.012(17)

Table S2. Chosen bond distances, angles and torsions of the [RuNO(3-CN-Py)$_2$(NO$_2$)$_2$OH].

Distance, Å		Angle, °		Torsions, °	
N5-O1	1.148(5)	Ru-5N-1O	171.6(3)	C1-N1-Ru-O2	17.7(3)
Ru-N5	1.769(3)	N5-Ru-2O	176.7(1)	C7-N2-Ru-O2	29.8(3)
Ru-N1	2.144(3)	N1-Ru-N5	93.7(1)	O3-N3-Ru-O2	27.1(4)
Ru-N2	2.122(3)	N2-Ru-N5	94.4(1)	O5-N4-Ru-O2	28.7(3)
Ru-N3	2.068(4)	N3-Ru-N5	88.3(1)	-	-
Ru-N4	2.056(4)	N4-Ru-N5	90.1(1)	-	-
Ru-O2	1.923(3)	-	-	-	-

The Hirshfeld surfaces were calculated using Crystal Explorer [7,8]. This program allows the normalized contact distance d_{norm} to be mapped onto the generated Hirshfeld surface. It is customary to map d_{norm} using a red–white–blue scheme, where red denotes close intermolecular contacts (negative d_{norm}), blue denotes longer contacts (positive d_{norm}) and white denotes intermolecular contacts equal to the van der Waals radii of atoms in contact (d_{norm} = 0). It is possible to obtain two-dimensional plots (fingerprint plots) from the surfaces mapped with d_{norm} values. Such plots are an invaluable asset in intermolecular interaction analysis since they serve as an executive summary of the quantity, nature and type of all intermolecular interactions at the same time.

The Hirshfeld surfaces of the complex showing intermolecular contacts are depicted in Figure S1. The red areas show the most pronounced interactions, where the strongest are formed by the oxygen atoms of nitrites and hydroxyl ligands. Contacts also can be observed for hydrogen atoms of 3-CN-Py, nitrogen atom of a cyanide group and for the aromatic rings of the 3-CN-Py ligands (Figure S1, *b*).

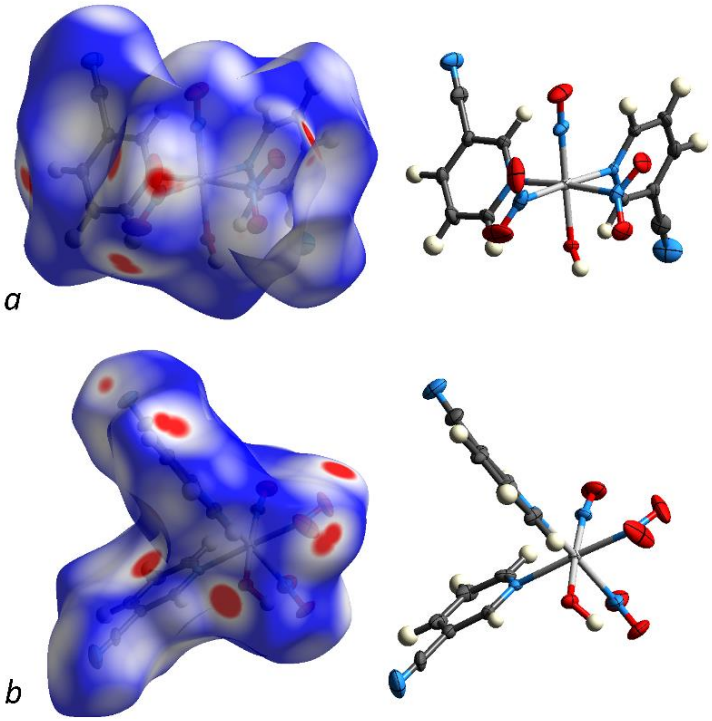

Figure S1. Three-dimensional Hirshfeld surface maps in selected projections (*a* and *b*), coloured by d_{norm} in the range -0.009–0.8 Å.

For the estimation of a relative contribution of the certain atoms to the whole intermolecular interactions, two-dimensional fingerprints are used and shown in Figure S2. The biggest contribution to the total Hirshfeld surfaces is found for O···H/H···O contacts (25.5%). This contacts are mainly formed by the O···H-C interactions and characterized as symmetric sharp edges in two-dimensional fingerprint plots (Figure S2, *b*). Surprisingly, the second biggest contribution to the Hirshfeld surfaces is made by the N···H/H···N interactions (18.1%), which are formed by the cyanide groups and hydrogen atoms of 3-CN-Py (Figure S2, *c*). Earlier was found, that cyanide group can form weak hydrogen interactions N···H-C with aromatic structures [9]. The C···O/O···C contacts are formed by the oxygen atoms of nitrite ligands and the aromatic rings of 3-CN-Py and contribute 16.7% to the total Hirshfeld surface (Figure S2, *d*). Described interactions (O···H/H···O, N···H/H···N and C···O/O···C) contribute 60.3% to the total Hirshfeld surface, the rest surface is formed by the H···H (15%), C···N/N···C (8.2%), O···N/N···O (6.9%) and C···H/H···C (6.9%) contacts. It was shown earlier, that stronger hydrogen bonds lead to the non-centrosymmetric structure and consequently to the enhancement of the second harmonic generation efficiency [10,11]. In current case we also observe sufficient contribution of the C···O/O···C, C···N/N···C and O···N/N···O interactions (the sum is 31.8%), which also could lead to the non-centrosymmetric structure formation.

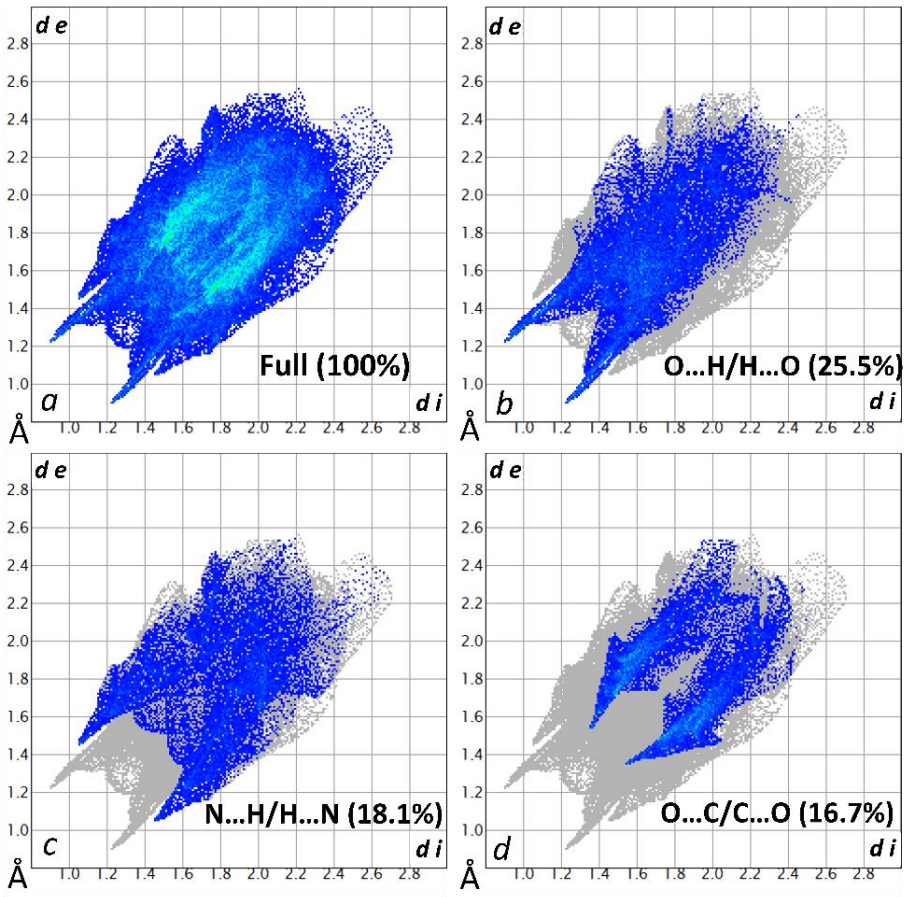

Figure S2. Selected two-dimensional fingerprint plots based on the Hirshfeld surfaces of the [RuNO(3-CN-Py)$_2$(NO$_2$)$_2$OH] for the full (*a*), reciprocal O···H (*b*), N···H (c) and O···C (c) intermolecular interactions.

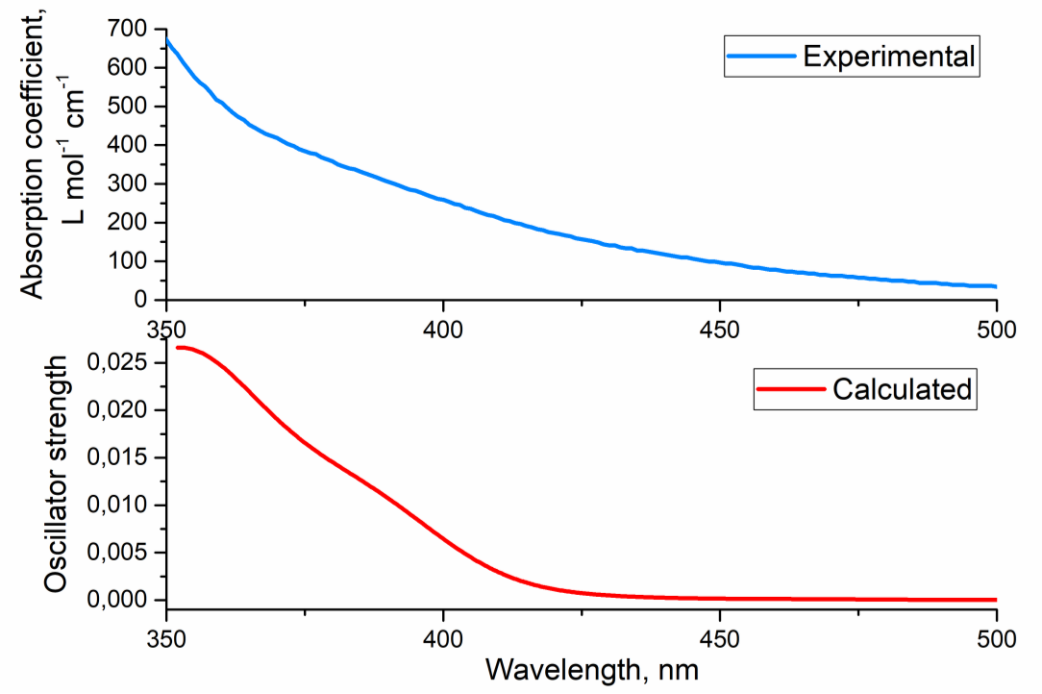

Figure S3. The experimental (blue curve, upper) and calculated spectra (red curve, lower) of [RuNO(3-CN-Py)$_2$(NO$_2$)$_2$OH] complex in acetonitrile.

Table S3. ν(NO)/ν(ON) stretching vibrations, MS1 populations and decay temperatures (T_d) of MS1→GS transformations of the nitrosyl ruthenium complexes with nitrite and N-donor heterocycle ligands.

Complex	$\nu(NO)_{GS}$, cm^{-1}	$\nu(ON)_{MS1}$, cm^{-1}	MS1, %	T_d, K	Ref.
$K_2[RuNO(NO_2)_4OH]$	1886	1722	16	187	[12]
$PyH[RuNOPy(NO_2)_2(ONO)OH]$	1882	1764	6	-	[13]
$NH_4[RuNOPy(NO_2)_3OH]$	1884	1770	6	206	[14]
$[RuNOPy_2(NO_2)_2OH]\cdot H_2O$	1883	1754	75	206	[15]
$[RuNO(\beta\text{-}Pic)_2(NO_2)_2OH]$	1878; 1863	1755; 1739	25	195	[16]
$[RuNO(\gamma\text{-}Pic)_2(NO_2)_2OH]$	1880	1751	40	193	[16]
$[RuNOPz_2(NO_2)_2OH]$	1890	1760	20	185	[17]
$[RuNO(inicEt)_2(NO_2)_2OH]$	1861	1734	30	205	[17]
$[RuNO(3\text{-}CN\text{-}Py)_2(NO_2)_2OH]$	1874	1748	10	199	Present work
$[RuNOPy_2(NO_2)(ONO)OH]$	1850	1757	8	-	[13]
$(NH_4)[RuNOPy_3(\mu\text{-}O)]_2(PF_6)_3$	1868	1730	19	-	[13]
$[RuNOPy_4OH](ClO_4)_2\cdot H_2O$	1876	1735	30	212	[18]

Table S4. Atomic coordinates of the calculated $[RuNO(3\text{-}CN\text{-}Py)_2(NO_2)_2OH]$ structure.

Ru	8.31687160	5.34144853	6.72972130
O	9.87556603	3.20512932	5.54508025
O	9.60115410	6.59738194	7.47346934
N	8.78629132	4.08606369	8.53199277
N	6.81929405	6.51054925	7.87666168
O	6.49906583	3.43149492	5.45195434
N	9.95348742	4.41011504	5.79950031
O	10.96826936	5.07236392	5.58640349
C	6.16488278	8.62056191	8.78958092
H	6.39362290	9.66850834	8.92900632
O	7.90597204	7.82104674	5.27115431
C	9.52031396	3.96784419	10.80195950
N	7.17536097	4.18319013	6.00379492
O	8.04740293	6.11032607	3.95317726
C	9.19234858	4.68987324	9.65339984
H	9.28478024	5.76674870	9.60941814
N	8.06057205	6.61689157	5.07111253
C	5.69929986	5.96658278	8.36589380
H	5.53699501	4.91251683	8.18621013
C	8.72568606	2.74455421	8.49718960
H	8.44310605	2.29999784	7.55281337
N	2.64525391	5.54321053	9.99678161
C	4.76240687	6.70759038	9.08456671
C	9.44242769	2.57224839	10.77154052
H	9.69706526	1.99322042	11.64958174
C	5.00271963	8.06939504	9.29845542
H	4.28940387	8.66679665	9.85106290
C	9.92794926	4.66103293	11.98537690
C	3.58755198	6.06616238	9.58793064

N	10.24644838	5.21554610	12.94430433
C	7.05296412	7.81904228	8.08321709
H	7.97373986	8.19657277	7.66338656
C	9.04525796	1.95883426	9.59520541
H	8.98829008	0.88160768	9.51664204
H	10.40982401	6.55249301	6.93158603

References

1 G. T. E. Velde, F. M. Bickelhaupt, E. J. Baerends, C. F. Guerra and S. J. A. V. A. N. Gisbergen, *J. Comput. Chem.*, 2001, **22**, 931.

2 K. Kim and K. D. Jordan, *J. Phys. Chem.*, 1994, **98**, 10089.

3 E. Van Lenthe and E. J. Baerends, *J. Comput. Chem.*, 2003, **24**, 1142.

4 E. van Lenthe, E. J. Baerends and J. G. Snijders, *J. Chem. Phys.*, 1993, **99**, 4597.

5 A. A. Mikhailov, D. V. Khantakova, V. A. Nichiporenko, E. M. Glebov, V. P. Grivin, V. F. Plyusnin, V. V. Yanshole, D. V. Petrova, G. A. Kostin and I. R. Grin, *Metallomics*, 2019, **11**, 1999.

6 W.-L. Chen, C.-M. Hsieh, L. Yang, C.-C. Hsu and S.-T. Lin, *Ind. Eng. Chem. Res.*, 2016, **55**, 9312.

7 F. L. Hirshfeld, *Theor. Chim. Acta*, 1977, **44**, 129.

8 M. A. Spackman and D. Jayatilaka, *CrystEngComm*, 2009, **11**, 19.

9 S. P. Platt, I. K. Attah, M. S. El-Shall, R. Hilal, S. A. Elroby and S. G. Aziz, *Phys. Chem. Chem. Phys.*, 2016, **18**, 2580.

10 S. Debrus, H. Ratajczak, J. Venturini, N. Pinçon, J. Baran, J. Barycki, T. Glowiak and A. Pietraszko, *Synth. Met.*, 2002, **127**, 99.

11 H. Athmani, C. Kijatkin, R. Benali-Cherif, S. Pillet, D. Schaniel, M. Imlau, N. Benali-Cherif and E.-E. Bendeif, *Acta Crystallogr. Sect. A Found. Adv.*, 2019, **75**, 107.

12 T. Woike and S. Haussühl, *Solid State Commun.*, 1993, **86**, 333.

13 G. A. Kostin, A. A. Mikhailov, N. V. Kuratieva, S. V. Tkachev, D. Schaniel and T. Woike, *Eur. J. Inorg. Chem.*, 2016, 4045.

14 G. A. Kostin, A. O. Borodin, N. V. Kuratieva, A. A. Mikhailov and P. E. Plusnin, *J. Mol. Struct.*, 2019, **1176**, 402.

15 G. A. Kostin, A. O. Borodin, A. A. Mikhailov, N. V. Kuratieva, B. A. Kolesov, D. P. Pishchur, T. Woike and D. Schaniel, *Eur. J. Inorg. Chem.*, 2015, **29**, 4905.

16 G. A. Kostin, A. A. Mikhailov, N. V. Kuratieva, D. P. Pischur, D. O. Zharkov and I. R. Grin, *New J. Chem.*, 2017, **41**, 7758.

17 G. A. Kostin, V. Vorobyev, A. A. Mikhailov and N. V. Kuratieva, *J. Mol. Struct.*, 2019, **1193**, 334.

18 V. Vorobyev, A. A. Mikhailov, V. Y. Komarov, A. N. Makhinya and G. A. Kostin, *New J. Chem.*, 2020, **44**, 4762.